Chemistry & Biology 13, 857–868, August 2006 ©2006 Elsevier Ltd All rights reserved DOI 10.1016/j.chembiol.2006.06.010

Folding of the Adenine Riboswitch

Jean-François Lemay,[1] J. Carlos Penedo,[2,3] Renaud Tremblay,[1] David M.J. Lilley,[2] and Daniel A. Lafontaine[1,*]
[1] Département de Biologie
Faculté des Sciences
Université de Sherbrooke
Québec, J1K 2R1
Canada
[2] Cancer Research UK Nucleic Acid Structure Research Group
The University of Dundee
Dundee, DD1 5EH
United Kingdom

Summary

The *pbuE* adenine riboswitch undergoes metal ion-dependent folding that involves a loop-loop interaction. Binding of 2-aminopurine to the aptamer domain strongly correlates with the ability of the loops to interact, and single-molecule FRET studies reveal that folding proceeds via a discrete intermediate. Folding occurs in the absence of adenine ligand, but ligand binding stabilizes the folded structure by increasing the folding rate and decreasing the unfolding rate, and it lowers the magnesium ion concentration required to promote the loop-loop interaction. Individual aptamer molecules exhibit great heterogeneity in folding and unfolding rates, but this is reduced in the presence of adenine. In the full riboswitch, the adenine binding domain fails to fold because of conformational competition by the terminator stem. Thus, riboswitch function should depend on the relative rates of ligand binding and the transcriptional process.

Introduction

Riboswitches are genetic control elements that are found in the 5′ untranslated region (UTR) of certain messenger RNAs of both prokaryotes and eukaryotes [1, 2]. These genetic switches are highly structured domains that are able to bind target cellular metabolites with high selectivity, resulting in conformational changes that ultimately modulate gene expression in the absence of proteins. Riboswitches are composed of two modular domains: a ligand binding aptamer and an expression platform. The most conserved region of known riboswitches is the aptamer domain, a receptor that specifically binds a given metabolite [3]. Expression platforms vary widely in sequence and structure, and they typically affect gene regulation by modulating the formation of Rho-independent transcriptional terminators or the sequestration of the Shine-Dalgarno sequences required for translation initiation [4].

The purine-specific class of riboswitches comprises the adenine and the guanine riboswitches, which are among the smallest riboswitches known to date. Despite the high structural similarity shown between these aptamers, they display very high specificity, discrimination, and affinity toward their respective cognate ligands, adenine and guanine (Figure 1) [3, 5]. In general, riboswitches repress their associated genes upon ligand binding, but like the glycine riboswitch, the *pbuE* adenine riboswitch is a rare type of "on" switch that activates gene expression upon ligand binding. The *pbuE* adenine riboswitch (formerly named *ydhL*) occurs upstream of a gene that encodes a purine efflux pump of *Bacillus subtilis*. It can adopt two different conformations [6, 7]. In the absence of adenine, the riboswitch adopts an "off state" structure, allowing the formation of a transcription terminator that is assumed to result in transcriptional attenuation (Figure 1A, "off" state). However, in the presence of adenine, an alternative structure is favored, resulting in the formation of an antiterminator stem (P1 stem). The formation of this stem thus permits transcription to take place (Figure 1A, "on" state). Interestingly, an adenine riboswitch that does not contain a transcription terminator is found in the 5′UTR of the *add* gene, which encodes for adenosine deaminase from *Vibrio vulnificus*. Instead, this riboswitch appears to modulate translation initiation through the formation of an alternative structure that sequesters the Shine-Dalgarno and initiation codon sequences in the absence of adenine [8]. Thus, purine riboswitches are able to regulate transcription or translation.

The adenine riboswitch aptamer is predicted to fold as a three-way junction in which the P1 stem is the only helical region showing some degree of conservation, presumably so it can interact with the expression platform domain [3]. Helices P2 and P3 are not conserved, but they undergo interaction between the loops. Three riboswitch aptamer structures have been determined by X-ray crystallography; the guanine-responsive riboswitch aptamer complexed with hypoxanthine was determined at a resolution of 1.95 Å [9], and a guanine complex was solved at 2.4 Å [8]. A *VV1*-adenine riboswitch aptamer variant was solved at 2.1 Å resolution [8]. In each complex, the fold of the RNA fragment is very compact, with many intricate tertiary interactions. Helices P1 and P3 form a coaxial stack, as often observed in three-way RNA junctions [10–13]. For each riboswitch, the metabolite is bound in a cavity, where it is sandwiched between four nucleotides to which it makes specific H bonding contacts. In particular, it was suggested [3] and subsequently shown [8, 14] that the specificity of the interaction with the ligand results from the formation of a Watson-Crick base pair with U65 (Figure 1A, circled nucleotide). Substitution of a cytosine for U65 converts the specificity to become guanine specific [3].

*Correspondence: daniel.lafontaine@usherbrooke.ca
[3] Present address: School of Physics and Astronomy, University of St. Andrews, North Haugh, St. Andrews, Fife, KY6 9SS, United Kingdom.

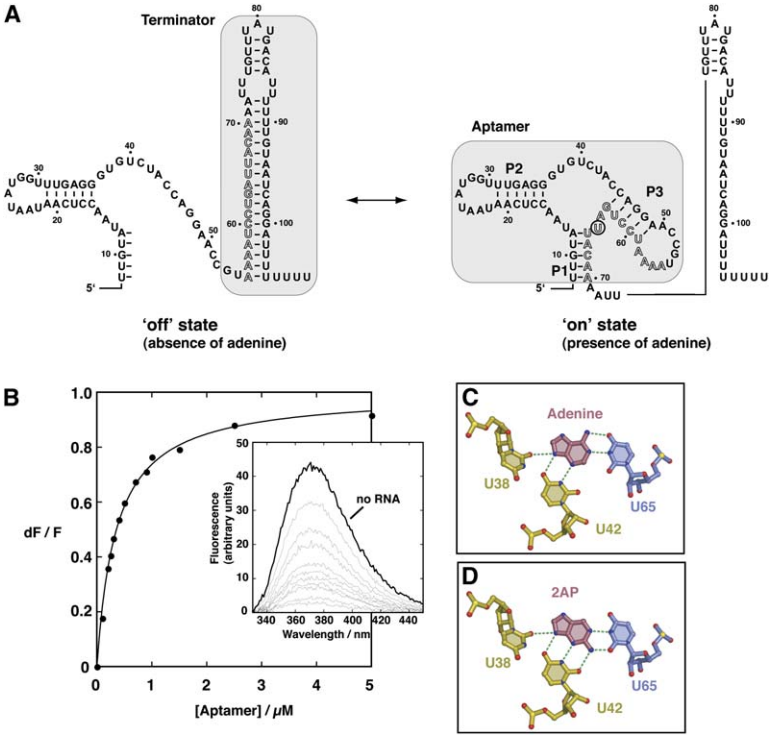

Figure 1. Binding of 2-Aminopurine to the *Bacillus subtilis pbuE* Adenine Riboswitch, Followed by Fluorescence Quenching

(A) Alternative base pairing of the *pbuE* adenine riboswitch associated with the "off" and "on" states. Shaded regions represent the transcription terminator stem ("off" state) and the aptamer structure ("on" state). The latter is expected to be stabilized by the binding of adenine. Outlined letters represent nucleotides that are involved in the formation of both the terminator and the aptamer structures.

(B) Normalized 2AP fluorescence intensity plotted as a function of aptamer concentration. Changes in fluorescence (dF) were normalized to the maximum fluorescence measured in the absence of RNA (F). The line shows the best fit to a simple binding model (see Experimental Procedures), yielding a K_{Dapp} of 354 ± 17 nM. The insert shows fluorescence emission spectra from 330 to 450 nm for each aptamer concentration. The bold line represents the 2AP fluorescence spectrum in the absence of RNA.

(C) Hydrogen bonds formed in the binding of adenine to the *Vibrio vulnificus* adenine riboswitch observed by X-ray crystallography [8].

(D) Predicted hydrogen bonds formed in the binding of 2AP to the riboswitch. Oxygen, nitrogen, and phosphorus atoms are colored red, blue, and yellow, respectively.

Recently, it has been found that the adenine and its structural isomer, 2-aminopurine (2AP), bind to the adenine-sensing aptamer with similar affinity [3, 15]. In this study, we have exploited this property and have used the fluorescence of 2AP to analyze the importance of the loop-loop interaction of the aptamer in isolation and in the context of the complete riboswitch that includes the expression platform. We show that the loop-loop interaction does not require the presence of the ligand, but that its formation is very important for ligand binding. Furthermore, the identity of the involved nucleotides is not critical for the formation of the structure. Using fluorescence resonance energy transfer (FRET) analysis, we show that the loop-loop interaction forms in the presence of low-micromolar concentrations of magnesium ions. Moreover, using single-molecule FRET studies, we have uncovered the existence of an intermediate state in the folding process of the loop-loop interaction structure. Interestingly, addition of adenine promotes the formation of the intermediate structure, suggesting that the ligand actively participates in the folding of the loop-loop interaction and, incidentally, in the folding process of the riboswitch aptamer domain. The latter characteristic is reminiscent of the roles of cofactors in protein folding in which the coordination of a cofactor prior to polypeptide folding can markedly accelerate the formation of the functional protein. Lastly, we show that the sequence context is important because, in the context of the adenine riboswitch, the presence of a stable terminator stem precludes the formation of the aptamer and thus inhibits ligand binding. These results indicate that the transcriptional process is key for riboswitch function and support the hypothesis that control of the riboswitch relies on the kinetics of ligand binding.

Results and Discussion

The *pbuE* Adenine Riboswitch Aptamer Binds 2-Aminopurine in an Apparently Identical Manner to Adenine

2-aminopurine (2AP) is a strongly fluorescent base that can be selectively excited in the presence of naturally occurring nucleobases [16]. 2AP is mostly used when incorporated in DNA or RNA molecules in place of a natural nucleobase. Its fluorescence is strongly quenched by stacking upon adjacent bases; thus, variation in the fluorescence intensity may be indicative of changes in the local environment of the fluorophore [16–21]. In the present study, the 2AP base has been used as the ligand of the adenine riboswitch aptamer, where it is expected that its intrinsic fluorescence will be affected by the formation of a complex with the aptamer. However, 2AP will be a good alternative to adenine as a ligand only if it is recognized in a similar manner to that of adenine. In order to validate this approach, we used in-line probing to investigate how similarly the adenine riboswitch aptamer recognizes adenine and 2AP. This assay exploits the inherent chemical instability of RNA under physiological conditions that is primarily due to the cleavage of phosphodiester linkages [22]. Spontaneous cleavage is more pronounced in unstructured single-stranded regions, because internucleotide linkages are free to adopt an in-line conformation that is precluded in the context of an A-form helix [22]. This assay has been extensively used to monitor conformational changes induced by external ligands on numerous mRNA leader regions [3, 5, 23–28]. Using this approach, we assessed whether adenine and 2AP lead to similar patterns of RNA degradation in the aptamer domain (see Figure S1A in the Supplemental Data available

with this article online), which might indicate a similar structure of the complexes. In the absence of ligand, several cleavage products were observed, all mapping to formally single-stranded regions. In the presence of adenine, the extent of cleavage in the core of the aptamer was found to be reduced, suggesting that the structure is more constrained upon ligand binding. Similar results have previously been observed by Breaker and coworkers [3]. Corresponding experiments were performed in the presence of 2AP, and a cleavage pattern that was identical to that obtained with adenine was observed. This finding suggests that both ligands are recognized in a similar manner.

It has been shown that the adenine riboswitch activates gene expression of a reporter gene in vivo in the presence of adenine [3], and we therefore investigated whether the riboswitch could also use 2AP to regulate gene expression in vivo. By using transcriptional fusions in which the 5′UTR sequence of the *pbuE* adenine riboswitch was fused to a β-galactosidase reporter gene, we observed that 2AP activated gene expression to a similar level to that obtained with adenine (see Figure S1B). Thus, our in vitro and in vivo results indicate that 2AP is recognized in an identical manner to adenine by the aptamer domain, and that it can be used by the adenine riboswitch to regulate gene expression in a biological context. This is also supported by very similar imino proton NMR spectra of adenine-sensing aptamers performed in the presence of adenine or 2AP [8].

The *pbuE* Adenine Riboswitch Aptamer Efficiently Quenches 2AP Fluorescence

We took advantage of 2AP fluorescence to monitor the ligand binding process between 2AP and the aptamer. The fluorescence intensity of 50 nM 2AP was measured as a function of increasing concentrations of RNA in the range of 0 to 5 μM. In the absence of the aptamer, a relatively high 2AP fluorescence signal was observed (Figure 1B, insert). As the concentration of the aptamer was increased, the 2AP fluorescence intensity progressively declined until it became almost totally quenched in the presence of 5 μM aptamer. The magnitude of the decrease suggests that 2AP becomes significantly stacked upon binding of the aptamer, consistent with the crystallographic structure of the aptamer-adenine complex, in which the bound adenine is completely surrounded by RNA, both along its periphery and with base stacking on both sides of the ligand [8]. Magnesium ions are essential for the ligand binding step given that no fluorescence quenching was detected in their absence, suggesting that the complex is not able to form in these conditions (data not shown). The fluorescence data were well fitted by a simple two-state binding model with no cooperativity (Figure 1B), and an apparent dissociation constant K_{Dapp} of 354 ± 17 nM was obtained. The fit is consistent with 1:1 stoichiometry between RNA and 2AP (see Experimental Procedures). Our value is in good agreement with that of Breaker and coworkers, who previously measured binding affinities of 300 nM for both adenine and 2AP [3, 15] by using in-line probing and 2AP fluorescence assays. Since adenine and 2AP have been shown to form approximately isosteric and isoenergetic base pairs with thymine [29], the ability of the aptamer domain to recognize 2AP in a manner similar to adenine can be explained by the formation of a base pair between 2AP and U65. The hydrogen bonding interactions between adenine and the surrounding bases in the aptamer-adenine complex crystal structure are represented in Figure 1C, showing the regular A-U base pair formed. Substitution of adenine by 2AP in this structure suggests that the aptamer should readily accommodate the exocyclic amine at the 2-position of the 2AP and permit a base-pairing interaction with U65 (Figure 1D). Thus, our results suggest that the adenine riboswitch aptamer recognizes 2AP and adenine in a similar manner, most probably indicating that the ligand is involved in a base-pairing interaction with U65.

Terminal Loops Are Important for Ligand Binding

Before crystal structures were available, loops P2 and P3 were known to be very well conserved, and a five base pair loop-loop interaction between them was suggested in the guanine riboswitch aptamer [5]. A mutational approach was used to analyze the importance of the loop-loop interaction for 2AP binding. First, two variants were made in which each of the P2 or P3 loop nucleotides involved in the proposed loop-loop interaction was changed for its respective counterpart (P2 comp. and P3 comp. variants, respectively, Figure 2A). No significant 2AP fluorescence quenching was detected for either mutant, indicating a complete loss of 2AP binding (Table 1). Similar conclusions have been observed in a previous study in the context of the guanine riboswitch [9]. Moreover, no binding was observed for magnesium concentrations up to 100 mM (data not shown). A third variant was made (P2 comp. + P3 comp.) in which both loop sequences were exchanged simultaneously, whereupon the 2AP binding activity was restored, albeit with a 28-fold reduced affinity compared to the natural molecule (Table 1, K_D^{rel} = 28). The observed restoration of 2AP binding suggests that the loop-loop interaction is required for ligand binding, and that this tertiary interaction occurs provided that the base pairing potential is maintained. Exchange of the entire P2 and P3 loops (P2 inv./comp. + P3 inv./comp.) resulted in 2AP binding affinity that was 2-fold higher than that of the natural molecule (K_{Dapp} = 166 nM, Table 1). The superior binding affinity of the latter variant, compared to the P2 comp. + P3 comp. variant, suggests that the precise sequence of the loops has an influence on 2AP binding. Taken together, our results suggest that the tertiary interaction between the P2 and P3 loops assists the formation of the complex formed between the aptamer and the 2AP ligand, presumably by stabilizing the folded structure of the aptamer.

The P2 and P3 loops can be viewed as auxiliary elements that stabilize the native structure of the adenine riboswitch aptamer by their interaction. RNA folding enhancers are increasingly found in RNA junction-containing molecules, as exemplified by the hammerhead [30, 31] and the hairpin [32, 33] ribozymes. However, unlike other RNA molecules in which a loop-loop interaction reduces the magnesium concentration required to achieve a native structure (in the hammerhead ribozyme, for example [30, 31]), the loop-loop interaction found in the aptamer domain is required for ligand binding to take place, and its loss cannot be compensated by a higher magnesium concentration. This suggests that

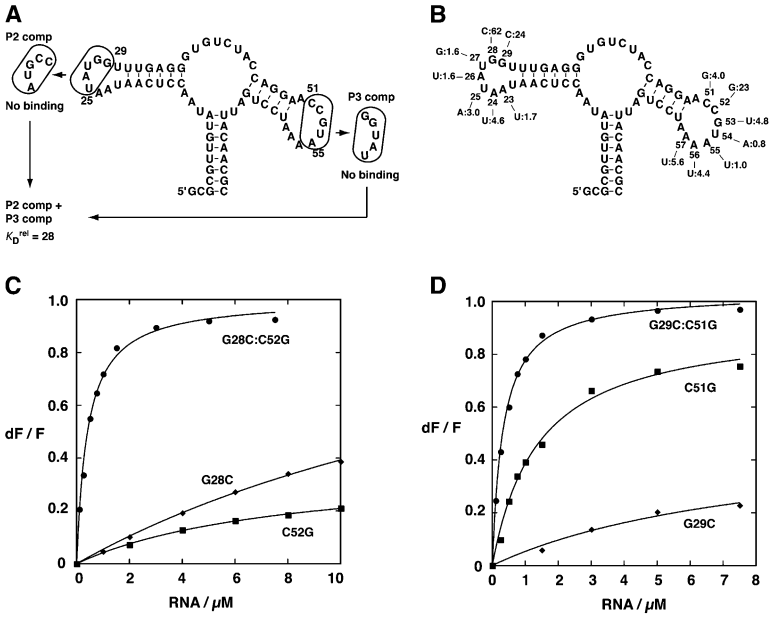

Figure 2. The Importance of Terminal Loops for the Formation of the Aptamer-Ligand Complex

(A) Disruption of the loop-loop interaction abolishes 2AP binding activity. The activity is recovered when the potential for the loop-loop interaction is restored. K_D^{rel} is the factor by which binding affinity is reduced for a given variant relative to the natural molecule, i.e., K_{Dapp} (variant)/K_{Dapp} (natural). A K_D^{rel} of 28 is obtained for the compensated variant, corresponding to a restoration of ligand binding by at least an order of magnitude.

(B) The importance of individual nucleotides for 2AP binding. Individual substitutions were performed in the P2 and P3 loops, generally replaced by the Watson-Crick complement (e.g., A23U).

(C) The importance of the G28-C52 base pair for 2AP binding. A plot of normalized 2AP fluorescence intensity as a function of RNA concentration is shown.

(D) The importance of the G29-C51 base pair for 2AP binding. A plot of normalized 2AP fluorescence intensity as a function of RNA concentration is shown.

the loop-loop interaction not only stabilizes a tertiary fold, but that it actively participates in the creation of the ligand binding site.

To explore this further, we performed an extensive mutational analysis of both the P2 and P3 loops to identify which nucleotides are important for 2AP binding (Figure 2B). Substitutions in positions 23–27 alter 2AP binding to some degree, with K_D^{rel} values ranging from 1.6 to 4.6 (Table 1). The small effect observed for A23U is not unexpected given the low evolutionary conservation observed at this position [5]. In contrast, G28C and G29C variants exhibit relatively weak 2AP binding (with relative dissociation constants K_D^{rel} = 62- and 24-fold, respectively), indicating that they are the most important nucleotides of the P2 loop. Similar analysis of the P3 loop revealed three categories of variant. The first category (U54A and A55U) exhibited almost no change in 2AP binding activity, while binding to the second category (C51G, G53U, A56U, and A57U) was reduced 4.0- to 5.6-fold. The largest effect was observed in the third class, C52G, with a K_D^{rel} of 23.

The crystal structure of the aptamer-adenine complex provides a structural basis for the interpretation of our results. The loop-loop interaction is maintained by the formation of several hydrogen bonds, mainly consisting of five base pairs [8]. Three of them are noncanonical pairs (A24•A57, U25•A56, A26•A55), while the remaining two are Watson-Crick pairs (G28-C52, G29-C51). Further interactions amongst the paired bases result in the formation of the two tetrad platforms A24•A57•G29-C51 and U25•A56•G28-C52. Substitutions of nucleotides contributing to the platforms generated aptamers with variable degrees of 2AP binding. Disruption of Watson-Crick base pairs generally led to a significant negative effect, while substitution of noncanonical ones did not affect 2AP binding severely. Perhaps surprisingly, the C51G change resulted in a small effect (K_D^{rel} = 4.0) given that C51 is involved in a Watson-Crick base pair. However, since the other three nucleotides of the tetrad platform make extensive hydrogen bonds, they may compensate for this change.

The weakest 2AP binding was observed when Watson-Crick base pairing positions G28, G29, and C52 were exchanged for their Watson-Crick counterparts. To investigate if 2AP binding defects observed for these positions were caused by the inability of the loop-loop interaction to form, aptamer molecules with compensatory changes were made. The doubly-substituted G28C:C52G variant exhibited 2AP binding very close to the natural riboswitch (K_D^{rel} = 1.9), showing that the identity of this base pair is not important for the formation of the loop-loop interaction or for the ligand binding activity. The base pair G28-C52 is part of the tetrad platform U25•A56•G28-C52, and, according to the crystal structure [8], two out of eight hydrogen bonds should be disrupted in the G28C:C52G variant. However, the affected hydrogen bonds are not involved in interactions between the loops, but are rather used in local interactions within each loop; this is probably why a relatively small effect is observed in 2AP binding to the G28C:C52G aptamer variant. A similar result was obtained (K_D^{rel} = 0.9, see Figure 3D) with the G29C:C51G variant, in which two out of seven hydrogen bonds connecting the loops would be disrupted. However, the presence of a Watson-Crick base pair between positions 29 and 51 is clearly sufficient to permit the formation of an aptamer-2AP complex. Overall, our results show that the identity of Watson-Crick base pairs present in the loop-loop interaction of the *pbuE* adenine riboswitch aptamer is not critical for ligand binding as long as the base pairing potential is maintained.

The Ligand Is Not Essential for the Formation of the Loop-Loop Interaction

Available X-ray crystal structures [8, 9] show that the loop-loop interaction is formed in the context of an aptamer-2AP complex. However, there are no data on the dependence of the loop-loop interaction on the

Table 1. Effect of Sequence Changes in the P2 and P3 Loops of the Aptamer Domain

Aptamer	K_{Dapp} (nM)	K_D^{rel}
Natural sequence	354 ± 17	(1)
Loop P2		
A23U	608 ± 105	1.7
A24U	1,631 ± 1,327	4.6
U25A	1,070 ± 99	3.0
A26U	562 ± 37	1.6
U27G	556 ± 36	1.6
G28C	22,107 ± 3,169	62
G29C	8,575 ± 4,038	24
P2 comp.[a]	n.d.	n.d.
P2 inv./comp.[b]	n.d.	n.d.
Loop P3		
C51G	1,402 ± 135	4.0
C52G	8,017 ± 703	22
G53U	1,704 ± 172	4.8
U54A	269 ± 19	0.8
A55U	351 ± 17	1.0
A56U	1,540 ± 138	4.4
A57U	1,976 ± 109	5.6
A58U	273 ± 10	0.8
P3 comp.[c]	n.d.	n.d.
P3 inv./comp.[d]	n.d.	n.d.
Loop-loop interaction		
G28C:C52G	415 ± 27	1.2
G29C:C51G	332 ± 15	0.9
P2 comp. + P3 comp.[e]	9,990 ± 749	28
P2 inv./comp.+ P3 inv./comp.[f]	166 ± 10	0.5

Apparent dissociation constants (K_{Dapp}) were measured under standard conditions for aptamer variants used in these studies. K_D^{rel} is the factor by which a given variant is impaired relative to the natural molecule, i.e., K_{Dapp} (variant)/K_{Dapp} (natural). The apparent dissociation constant of weak 2AP binding variants (e.g., K_{Dapp} > 100 μM) is not determined (n.d.).

[a] U25A, A26U, U27G, G28C, and G29C mutations were performed simultaneously.

[b] Nucleotides A23–G29 replaced with C51–A57; this effectively creates two P3 loops in the same molecule.

[c] C51G, C52G, G53U, U54A, and A55U mutations were performed simultaneously.

[d] Nucleotides C51–A57 replaced with A23–G29; this effectively creates two P2 loops in the same molecule.

[e] Nucleotides A23–G29 relocated to positions 51–55, and nucleotides C51–A55 relocated to positions 23–29.

[f] Nucleotides A23–G29 replaced with C51–A57, and nucleotides C51–A57 replaced with A23–G29.

presence of the ligand. We hypothesized that if the interaction between the loops is formed in the absence of any ligand, the guanine nucleotides at positions 28, 29, and 53 should be involved in the loop-loop interaction and should not be cleaved by the single-stranded, guanine-specific nuclease RNase T1. A partial RNase T1 assay was performed to probe the environment of guanine bases located in the P2 (G28 and G29) and P3 (G53) loops. All predicted single-stranded guanines, except G37, are strongly cleaved by RNase T1 in the absence of magnesium ions (Figure 3A). The latter is located at the end of the P2 stem and has been found in the crystal structures of the adenine-sensing domain [8] and the G box aptamer [9] to form a Watson-Crick base pair with C44, potentially offering protection against RNase T1 cleavage. When the experiment was repeated in the

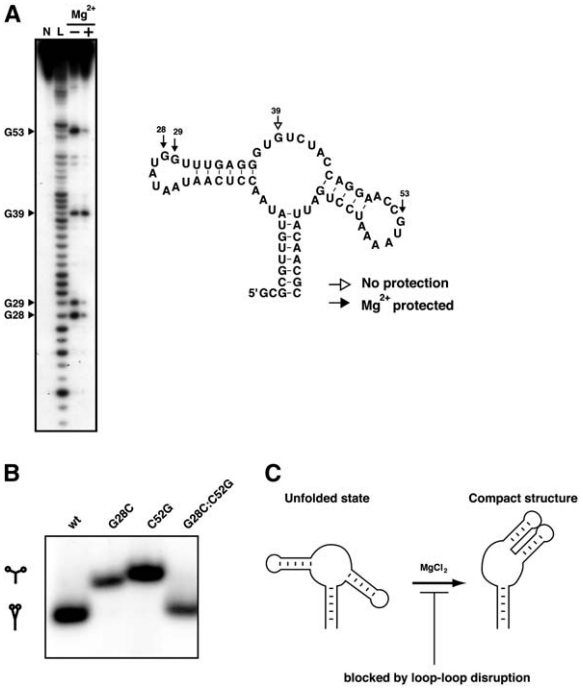

Figure 3. The Loop-Loop Interaction Occurs in the Absence of Ligand

(A) Partial digestion of [5′-^{32}P]RNA by RNase T1 shows that the P2 and P3 loops are protected from cleavage in the presence of 10 mM magnesium. Positions of strong cleavage are identified on the left. Lane N contains unreacted RNA, while lane L contains RNA that was subjected to partial alkaline digestion. A summary of RNase T1 reactivity is shown on the right. Guanine bases that are protected from RNase T1 cleavage in the presence of magnesium are indicated by black arrows.

(B) Nondenaturing gel electrophoresis of the natural (wt) and three aptamer loop variants in the presence of 10 mM magnesium ions. Loop variants (G28C:C52G) exhibit retarded electrophoretic migration rates, while the mobility is largely restored for the double variant (G28C:C52G).

(C) Interpretation of the results of RNase T1 digestion and native electrophoretic migration rates shown in (A) and (B). A compact structure is adopted in the presence of magnesium ions, correlating with the loop-loop interaction.

presence of magnesium ions, a significant reduction of cleavage products was observed in both the P2 and P3 loops, while cleavage at G39 remained constant (summarized in Figure 3A). These results suggest that the loop-loop interaction forms in the presence of magnesium ions alone, without a requirement for ligand binding. No additional changes were observed in the presence of adenine or 2AP (data not shown).

The magnesium ion-induced interaction between the loops was also studied by native gel electrophoresis. This technique can be used to study global conformational changes in nucleic acids because a compact structure generally migrates faster than a more extended one [34–37]. We reasoned that aptamers with a loop-loop interaction should have a compact structure—and thus a fast migration rate—when compared to variants compromised in the interaction. The migration pattern of the natural aptamer was compared to those of two selected loop variants (Figure 3B). The electrophoretic mobility of these two variants is markedly slower than that of the natural molecule, suggesting

that disruption of the loop-loop interaction leads to a more extended structure (Figure 3B). However, when both mutations were introduced in the same molecule, faster electrophoretic mobility was restored, suggesting that the loop-loop interaction is formed and thereby confers a compact structure on the aptamer. These experiments were repeated in the absence of magnesium ions, and no variation in migration was observed (data not shown). Taken together, our results suggest a model in which a loop-loop interaction forms in the presence of magnesium ions and does not require the presence of ligand (Figure 3C). However, we cannot determine the role of the loop-loop interaction in the organization of the ligand binding site at this point.

Magnesium-Induced Formation of the Loop-Loop Interaction Studied by Fluorescence Resonance Energy Transfer

FRET is especially informative in the study of the conformation of branched nucleic acids in solution, providing quantitative data both on the global structure and conformational transitions [38]. In this approach, donor and acceptor fluorophores are attached at known positions in the molecule. Efficiency of energy transfer (E_{FRET}) between them is inversely related to the sixth power of their separation (R) [39]:

$$E_{FRET} = (1 + [R/R_0]^6)^{-1}, \quad (1)$$

where R_0 is the Förster length for the fluorophores used. A value of 55.7 Å was previously determined for the fluorescein-Cy3 combination [40]. Fluorophore positions were carefully chosen to avoid interference with the loop-loop interaction. Nucleotide positions U27 and U53 are not strongly conserved and are exposed to the solvent in the crystal structure of the *VV1* aptamer [8]. The *VV1* aptamer was therefore used for this study, and fluorescein and Cy3 fluorophores (donor and acceptor respectively) were attached at positions 27 and 53 through the 5-position of the uracil rings (Figure 4A) by using a combination of chemical and enzymatic methods [41, 42]. The structures of the different purine riboswitch aptamers are very similar in the crystal [8, 9, 43]; thus, conformational conclusions drawn from the *VV1* variant should be transferable to *pbuE*.

Since the fluorophores are located at the ends of the P2 and P3 stem-loops (Figure 4A), it was expected that folding involving the loop-loop interaction would result in a large increase in energy transfer. The FRET efficiency was measured in the steady state as a function of magnesium ion concentration (Figure 4B). Addition of magnesium ions in the micromolar range results in a very large increase in FRET, consistent with induction of the loop-loop interaction. The data have been fitted to a simple two-state model that assumes an all-or-none conformational transition induced by the binding of magnesium ions. The proportion of folded aptamer (α) is given by:

$$\alpha = K_A \cdot [Mg^{2+}]^n / (1 + K_A \cdot [Mg^{2+}]^n), \quad (2)$$

where K_A is the apparent association constant and *n* is a Hill coefficient. From these, we can calculate the magnesium ion concentration ($[Mg^{2+}]_{1/2}$) at which the transition is 50% complete. Values of *n* were obtained that were within experimental error of unity under all conditions, indicating noncooperative binding. In the absence of adenine, the data fitted $[Mg^{2+}]_{1/2} = 22\ \mu M$ and $n = 1.1 \pm 0.1$, showing that the apparent affinity for magnesium ions is relatively high. The experiment was repeated in the presence of 50 μM adenine. A similar transition was observed and fitted to the two-state model to give $[Mg^{2+}]_{1/2} = 12\ \mu M$, $n = 1.0 \pm 0.1$. The 2-fold decrease in half-magnesium concentration observed in the presence of adenine shows that the formation of the loop-loop interaction is assisted to a small degree by the binding of adenine. In the crystal structure, the bound adenine is sandwiched between the J23 region and the P1 stem [8]. A series of stacking interactions are present at the base of the P2 stem involving the base pairs G37-C44, U13-A43, and U38:U42 (Figure 4C, shaded region). The U38:U42 mispair interacts directly with the bound adenine. Probing experiments [3, 5] have suggested that the core of the aptamer is rather flexible in the absence of adenine, but that it becomes more constrained

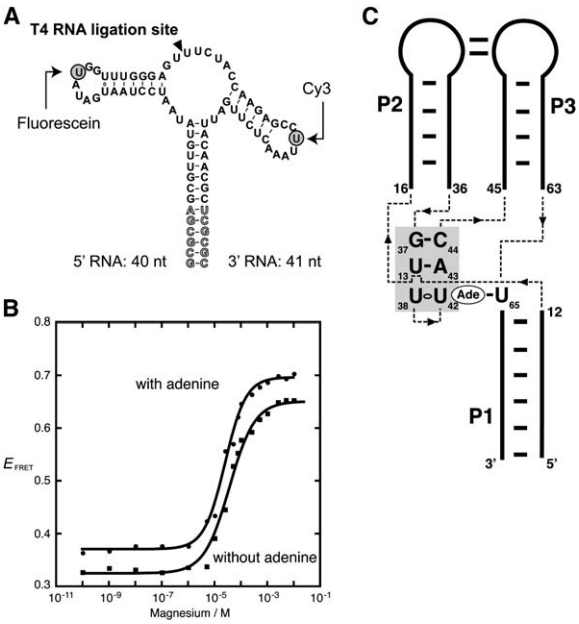

Figure 4. Loop-Loop Interaction Studied by Ensemble Steady-State FRET

(A) Secondary structure of the adenine riboswitch binding domain with donor (fluorescein) and acceptor (Cy3) fluorophores attached in the loops at the shaded positions by conjugation to 5′-amino-allyl uridine nucleotides. The RNA sequence is based on the *VV1* aptamer variant since the fluorophore positions have been chosen in light of the crystal structure of this aptamer [8].

(B) Plot of the efficiency of FRET as a function of magnesium ion concentration in the absence (circles) or the presence (squares) of 10 μM adenine. FRET efficiency increased markedly with the addition of the divalent metal ion, corresponding to an ion-induced folding that results in a shortening of the distance between the loops. The experimental data were fitted (lines) by regression to a simple two-state model in which the binding of metal ions to RNA induces a structural change.

(C) Schematic representing tertiary interactions between the core region and the bound adenine. The drawing is adapted from [8] and [43]. Only selected nucleotides are shown. Solid and dotted lines represent the backbone of the molecule, and Watson-Crick base pairs are shown by short bars. A deviation in the backbone is shown under nucleotide 13 to indicate that it is actually part of the strand. Black arrows indicate the polarity of the backbone. The bound adenine (Ade) is highlighted.

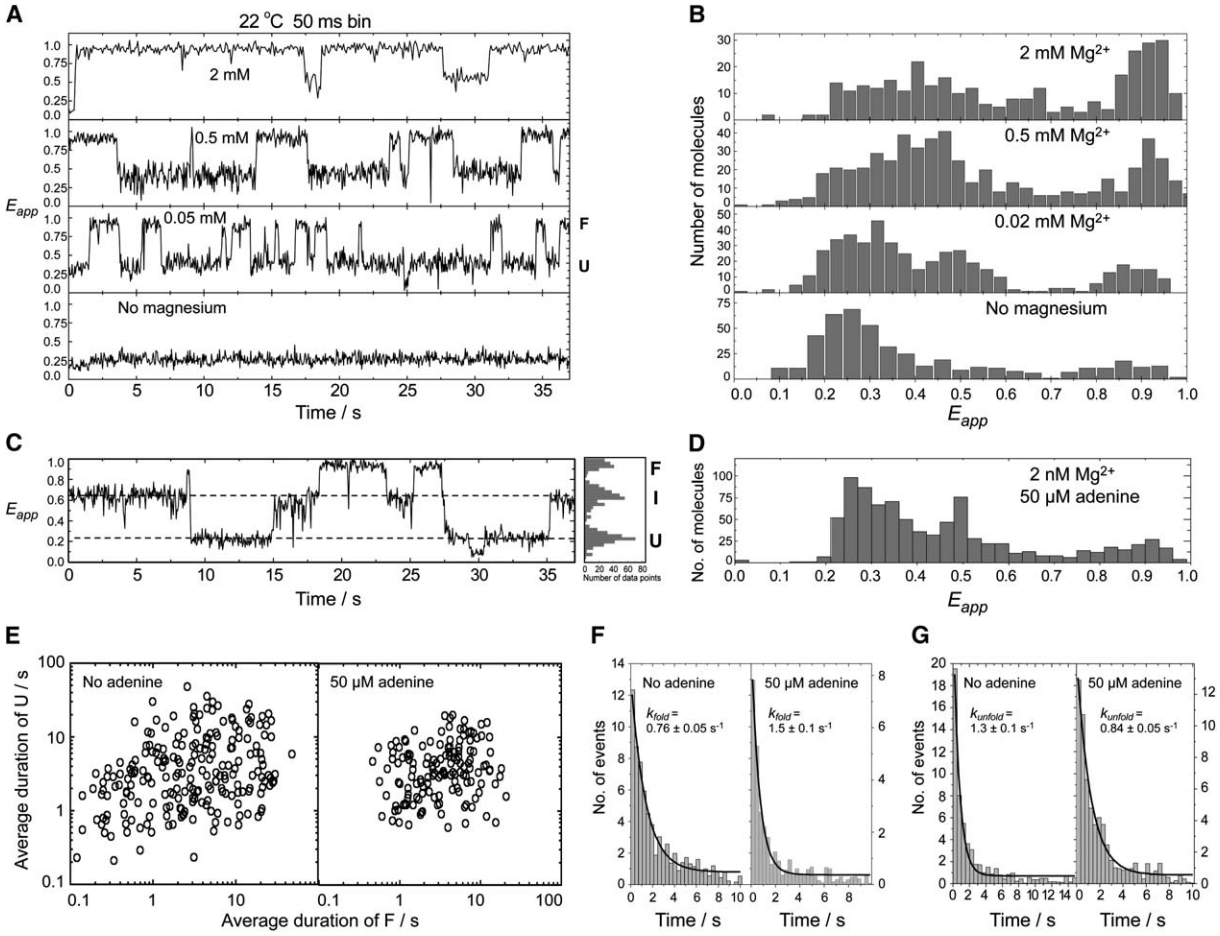

Figure 5. Loop-Loop Interaction Studied by Single-Molecule FRET

(A) Time records of FRET efficiency (50 ms integration time) as a function of elapsed time for single aptamer molecules at various magnesium ion concentrations.

(B) Histograms of FRET efficiency summed over multiple single molecules at different magnesium ion concentrations. Individual time traces were manually filtered to remove the contribution from fluorophore blinking and photobleaching events.

(C) An intermediate folding state in the adenine aptamer. FRET trace and histogram for a single molecule (50 ms integration time) in the presence of 0.02 mM Mg^{2+} clearly showing interconversion between three states, **U** ($E_{app} \approx 0.25$), **I** ($E_{app} \approx 0.5$), and **F** ($E_{app} \approx 0.9$). A fluorophore blinking event has occurred at 30 s.

(D) FRET histogram obtained in the presence of 2 nM Mg^{2+} and 0.05 mM adenine showing three peaks corresponding to the **U**, **I**, and **F** states.

(E) Heterogeneity between molecules in the folding and unfolding rates of the aptamer domain. Scatter plot showing the average duration of **U** and **F** states for 210 molecules in the presence of 0.5 mM Mg^{2+} and up to 100-fold variation in both rates. The spread of rates becomes significantly narrowed in the presence of adenine (150 molecules).

(F) Dwell time histograms of the unfolded states (**U** and **I**) in the presence of 0.5 mM Mg^{2+} with and without 50 µM adenine. The data have been fitted to single exponential decay functions to give the rate of folding (k_{fold}).

(G) Dwell time histograms of the folded state (**F**) in the presence of 0.5 mM Mg^{2+} with and without 50 µM adenine. The data have been fitted to single exponential decay functions to give the rate of unfolding (k_{unfold}).

in the presence of ligand. Ligand-induced stabilization of the core would be expected to facilitate the loop-loop interaction.

FRET Analysis of Single Aptamer Molecules Reveals a Discrete Folding Intermediate

We have further analyzed the ion-induced folding of the adenine riboswitch aptamer domain by using FRET in single riboswitch molecules. These experiments can provide information that is difficult to obtain from ensemble measurements, including the identification and correlation of folding intermediates [44, 45] and the extent of dynamic heterogeneity in the population [46–52]. In the current experiments, we have employed a similar *VV1* aptamer construct to that used for ensemble FRET experiments, except that the fluorescein has been replaced by Cy5. The molecules were tethered to a quartz slide via biotin that was attached to the 5′ terminus of the P1 stem and were studied by using a wide-field total internal reflection (TIR) microscope (see Experimental Procedures). Single-molecule time records and apparent FRET efficiency (E_{app}) histograms have been obtained for different magnesium ion concentrations (Figures 5A and 5B, respectively). States with low (E_{app} = ~0.25) and very high (~0.9) FRET efficiency are seen, in agreement with the steady-state FRET results, with frequent transitions between the two. The relative duration of these two states exhibits

a strong dependence on magnesium ion concentration (Figure 5A). In the absence of ions, the aptamer domain remains mostly in the low-FRET state, and a corresponding major peak is observed at low FRET efficiency in the histogram. As the magnesium concentration is increased, the low-FRET state decreases in population, and the time traces contain many transitions between low and high-FRET states. Above 2 mM magnesium ions, the aptamer molecules exist mostly in the high-FRET state until fluorophore photobleaching occurs. Ensemble FRET measurements indicated that the aptamer is mostly folded at this magnesium ion concentration; therefore, we assign the high-FRET state to the folded structure (Figure 5A, termed **F**). Similarly, the low-FRET state, termed **U**, clearly corresponds to the unfolded conformation.

Detailed analysis of selected time records collected at magnesium ion concentrations below 50 μM reveals that the unfolded state is actually a mixture of at least two different states (Figure 5C). One state has an E_{app} of ~0.25, which is similar to that observed in the absence of magnesium, while the other state, termed **I**, has an E_{app} of ~0.55. At magnesium ion concentrations higher than ~50 μM, the interconversion between **U** and **I** is too fast to be resolved by our TIR microscope (with a time resolution of 16 ms), and this fast interconversion accounts for the increase in the mean FRET efficiency of the low-FRET state observed in the histograms with increased magnesium ion concentration (Figure 5B). The existence of this intermediate state in the folding of the adenine aptamer was not detected in the ensemble FRET studies; it is a new finding afforded by the discrimination of single-molecule measurements. Transitions between the three states (**U**, **I**, and **F**) could be observed within single aptamer molecules, most easily at magnesium ion concentrations below the $[Mg^{2+}]_{1/2}$ obtained in ensemble studies (e.g., 20 μM Mg^{2+}) (see Figure S2). To identify any possible role(s) of this intermediate state **I** in the binding of adenine, single-molecule FRET measurements were repeated in the presence of 50 μM adenine and 2 nM magnesium ions. Despite the very low magnesium ion concentration, the three states were again observed (Figure 5D), indicating that the formation of the **I** state is promoted by the binding of adenine even at ionic conditions at which the loop-loop interaction is disfavored. This is consistent with the ensemble FRET results showing that the presence of adenine results in a modest reduction of the magnesium ion concentration required for folding into the high-FRET state (Figure 4B). Analysis of 846 single-molecule traces at 0.5 mM magnesium ions reveals that only 6% of them show apparently direct transitions between the unfolded **U** and the folded **F** state, with the remaining 94% involving the intermediate at some stage of the folding process. This suggests that the **I** state is likely to be an obligate intermediate in the folding process of the aptamer.

A surprising property of a number of different RNA species emerging from single-molecule studies has been that individual molecules can differ markedly and persistently in their folding and unfolding rates [47, 52, 53]. We measured the average dwell times of the **F** and **U** states for 200 aptamer molecules in the presence of 0.5 mM magnesium ions. A two-dimensional scatter plot of the mean dwell times (Figure 5E) reveals a 100-fold variation for both folding and unfolding rates, particularly for the duration of the folded state. Interestingly, the addition of 50 μM adenine significantly reduced this heterogeneity, with a 10-fold decrease in the spread of both rates. Dwell time histograms were plotted for folded and unfolded states in the presence of 0.5 mM magnesium ions, corrected by a weighting factor inversely proportional to the number of transitions in each molecule in order to avoid bias toward fast-fluctuating molecules (Figures 5F and 5G). The data were fitted to single-exponential functions, giving rate constants for docking of k_{fold} = 0.76 ± 0.05 s^{-1} and undocking of k_{unfold} = 1.3 ± 0.1 s^{-1} in the absence of adenine. In the presence of 50 μM adenine, these changed to k_{fold} = 1.5 ± 0.1 s^{1} and k_{unfold} = 0.84 ± 0.05 s^{-1}, showing that the stabilization of the folded state by the ligand results from changes to both folding and unfolded rates.

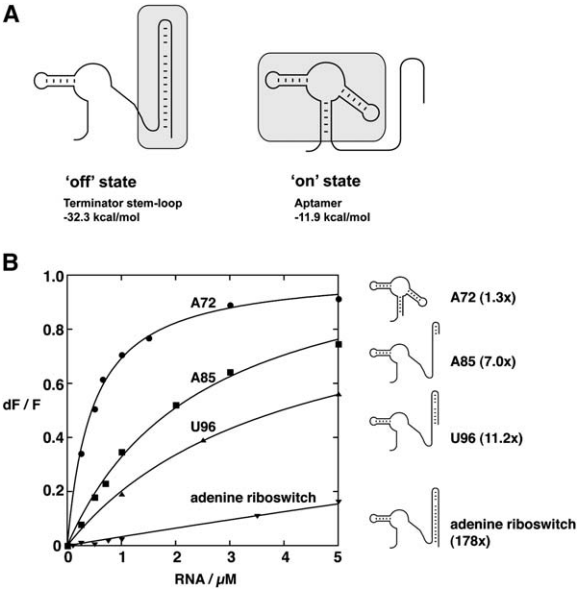

Figure 6. Conformational Competition between the Folding of the Aptamer Domain and the Terminator Stem-Loop in the Complete Riboswitch Studied by 2AP Binding

(A) Schematic showing two mutually exclusive secondary structures occurring in the absence ("off" state) or in the presence of adenine ("on" state). Shaded regions represent the fully formed terminator stem and the aptamer domain. The relative free energies of the terminator stem and the aptamer were calculated with the program *mfold*. The value associated to the aptamer is given as an estimate since additional tertiary interactions could have an influence on the free energy of the molecule.

(B) Plot of relative fluorescence intensity of 2AP as a function of RNA concentrations. The data have been fitted (lines) to a simple binding model (see Experimental Procedures). The potential extent of terminator stem formation is shown schematically for each variant on the right, with the associated K_D^{rel}.

The Expression Platform Negatively Influences the Formation of the Aptamer

In the complete adenine riboswitch, the adenine-sensing aptamer is directly 5′ to an additional structural domain called the expression platform (Figure 1). The latter is a potential stem-loop that can act as a transcriptional terminator. In the absence of adenine, the expression of a reporter gene is very low, and this is attributed to the

formation of the terminator, resulting in the "off" state (Figure 6A) [3]. The stretch of nucleotides from position 55 to position 70 can participate in two mutually exclusive secondary structures. They can either form the terminator stem-loop or stems P1 and P3 of the aptamer region. A secondary structure analysis performed using the program *mfold* predicts a free energy of −32.3 kcal/mol for the terminator stem and one of −11.9 kcal/mol for the aptamer.

We analyzed the conformation of the aptamer in the context of the complete adenine riboswitch by using the 2AP fluorescence assay (Figure 6B). This shows that the riboswitch has a very low 2AP binding affinity (K_D^{rel} = 178, Figure 6B), probably resulting from an inability of the aptamer to fold with the complete terminator present. Under our experimental conditions, the terminator stem should be the more stable structure, thereby precluding the formation of the aptamer structure. If so, decreasing the stability of the terminator helix should bias the equilibrium to favor the "on" state, in which the aptamer is able to fold and bind 2AP. Three deletion variants resulting in progressively shorter potential stem-loop structures were examined for their ability to quench 2AP fluorescence. Truncation after A72 removes the entire terminator while still allowing the aptamer to fold; this exhibits strong 2AP binding (K_D^{rel} = 1.3, Figure 6B) similar to that of the isolated aptamer. A construct derived by truncation after A85, thus making a riboswitch consisting of only four base pairs of the terminator stem, gave a substantial decrease in 2AP binding affinity (K_D^{rel} = 7.0). Thus, even the formation of a terminator stem of only four base pairs is able to alter the equilibrium between the "on" and "off" riboswitch conformers. Deleting a portion from U96 halves the length of the stem-loop, producing a K_D^{rel} of 11.2. Taken together, these results demonstrate that the greater the potential stability of the terminator stem, the lower the stability of the folded conformation of the aptamer domain. Very recently, in-line probing experiments have shown that adenine is unable to induce structural changes in the complete adenine riboswitch [15]. Collectively, the data show that the adenine riboswitch is unable to efficiently bind 2AP and adenine, most probably as a result of the stability of the competing terminator stem.

The Transcription Process Has a Central Role in Riboswitch Function

Our work shows that the loop-loop interaction is very important for the binding of adenine. However, we have also shown that sequence context (especially the presence of the expression platform) can strongly influence the loop-loop interaction and, thus, the binding of the adenine ligand. In particular, the dependence of aptamer folding on the length of the terminator sequence suggests that the relative rates of transcription and adenine binding will be critical in the regulation. In the present case, the binding of adenine has to occur during a relatively precise moment during the transcriptional process for the regulation to occur. Adenine must bind the RNA when the aptamer domain is fully transcribed, but before the transcription of the expression platform, since the aptamer structure will be disrupted by the formation of the terminator stem ("off" state). Intervention of transcriptional pause sites between the aptamer and the expression platform could give the aptamer additional time to bind to the ligand before the formation of the platform and, thus, can play a key role in the regulation process; these have been found in other systems [54–56]. Two such strategic pause sites have been suggested for the adenine riboswitch [15] but require experimental investigation. It is expected that the complex formed by the aptamer and the ligand will inhibit formation of the terminator structure where the "on" state remains folded in the context of the completely transcribed riboswitch to allow for gene expression. Additional factors such as the time needed for the polymerase to move beyond the transcription terminator and the concentration of cellular ribonucleoside triphosphates could also affect the equilibrium between conformational states.

Significance

The adenine riboswitch aptamer domain undergoes a dynamic, metal ion-induced folding process, with a degree of induced fit by the adenine ligand. The folding process involves the formation of an intimate interaction between the two terminal loops, and sequence variations that interfere with the interaction inhibit the global folding of the aptamer. Single-molecule FRET analysis reveals that the folding pathway includes a discrete intermediate state and provides further evidence for assistance by the binding ligand. Folding and unfolding rates exhibit pronounced heterogeneity between different molecules, but the distribution of rates is significantly narrowed in the presence of adenine. In the complete riboswitch, the conformational competition between the mutually exclusive aptamer and terminator stem-loop structures is significantly biased toward the terminator. Control of gene expression is therefore likely to depend on the relative rates of ligand-assisted folding of the aptamer and the rate at which the synthesis of the complete riboswitch is achieved by transcription.

Experimental Procedures

Purification of DNA Oligonucleotides

Oligonucleotides were purchased from Sigma Genosys (Canada). They were purified by electrophoresis in 10% or 20% polyacrylamide gels containing 7 M urea, electroeluted into 8 M ammonium acetate, recovered by ethanol precipitation, and dissolved in water.

Transcription of RNA

RNA was transcribed from a double-stranded DNA template by using T7 RNA polymerase [57]. Templates for transcription of adenine riboswitches were made by recursive PCR from purified synthetic DNA oligonucleotides. RNA was purified by denaturing PAGE and was recovered as described for DNA oligonucleotides. Templates for aptamers were made from DNA oligonucleotides (500 pmol) containing the aptamer and the T7 promoter sequence, which were incubated in a 20 μl mixture containing 10 mM Tris-HCl (pH 7.5), 10 mM $MgCl_2$, 50 mM KCl. This was denatured by heating at 95°C for 1 min and was allowed to cool slowly to 37°C. The in vitro transcription reactions were carried out by using the formed partial duplex as a template under the same conditions described for the production of the full-length riboswitch. All transcribed RNA species begin with a 5′-GCG sequence in order to minimize the 5′ heterogeneity of the RNA population [58]. The following oligos were used (all sequences are written in the 5′ to 3′ direction): aptamer, GCGCGUU

GUAUAACCUCAAUAAUAUGGUUUGAGGGUGUCUACCAGGAACC GUAAAAUCCUGAUUACAACGC; adenine riboswitch, GCGUUGUA UAACCUCAAUAAUAUGGUUUGAGGGUGUCUACCAGGAACCGUA AAAUCCUGAUUACAAAAUUUGUUUAUGACAUUUUUUGUAAUCAG GAUUUUUUUU. Variants were also prepared with the sequence changes indicated in the text.

2AP Fluorescence Binding Assay

Fluorescence spectroscopy was performed on a Quanta Master fluorometer. All data were collected at 25°C in 10 mM $MgCl_2$, 50 mM Tris-HCl (pH 8.3), and 100 mM KCl. Spectra were corrected for background, and intensities were determined by integrating the data collected over the range 330–450 nm. Excitation for 2-aminopurine was excited at 300 nm to obtain a good separation between the Raman and fluorescence peaks.

The relative quenching of 2AP fluorescence was determined by monitoring the fluorescent emission of a fixed concentration of 2AP (50 nM) and titrating the concentration of RNA. If the total RNA concentration is in large molar excess relative to 2AP, then it can be assumed that the concentration of free RNA is similar to the concentration of total RNA molecules. The binding can thus be described by the equation:

$$dF/F = (1 - a)[RNA]/(K_{Dapp} + [RNA]), \quad (3)$$

where dF is the change in fluorescence intensity, F is the fluorescence intensity in the absence of RNA, and K_{Dapp} is the apparent dissociation constant. The parameter *a* is a dimensionless constant proportional to the ratio of the quantum yields of 2AP both in the complex and free in solution. *a* is also less than unity, as the quantum yield of 2AP free is higher than in the complex. The equation assumes a simple 1:1 stoichiometry between the RNA and 2AP, as has been reported in the various crystal structures of aptamer-ligand complexes [8, 9]. The reported errors are the standard error in the fitting, which is thus assumed to be approximated by the standard deviation of the points from the fitted curve [59, 60].

Preparation of Dual-Labeled Fluorescent Aptamer Molecules

The aptamer molecule was assembled from oligonucleotides of the following sequences (all written in the 5′ to 3′ direction): 5′ strand, biotin-GCGCGAGCGUUGUAUAAUCCUAAUGAUAUGGUUUGGGA GU; 3′ strand, UUCUACCAAGAGCCUUAAACUCUUGAUUACAACG CUCGCGC. The RNA molecules were purchased from Dharmacon (Boulder, CO) with 5′-amino-allyl uridines nucleotides at defined positions (underlined nucleotides). Succinimidyl ester derivatives of fluorophores (Invitrogen) were used according to the manufacturer's protocol for the specific labeling of fluorescein/Cy5 and Cy3 dyes on the 5′ and 3′ RNA strands, respectively. Fluorescent RNA conjugates were deprotected and purified as described previously [61]. Purified RNA strands were annealed by heating a mixture (molar ratio 1:1) to 80°C in 10 mM HEPES (pH 7.5), 50 mM NaCl and slowly cooling it to room temperature. T4 RNA ligase (New England BioLabs) was then added to the reaction, and samples were incubated for 4 hr at 37°C. Full-length ligated RNA molecules were purified by denaturing polyacrylamide gel electrophoresis and electroelution. The RNA was precipitated with ethanol and redissolved in water. RNA concentration was measured by absorption of light at 260 nm.

Fluorescence Intensity Measurements in the Steady State

Fluorescence intensities were measured in the steady state by using an SLM-Aminco 8100 fluorimeter, and spectra were corrected for lamp fluctuations and instrumental variations as described [62]. Polarization artifacts were avoided by setting excitation and emission polarizers crossed at 54.74°. Values of E_{FRET} were measured by using the acceptor normalization method [63, 64]. The FRET experiments were performed with the 5′ RNA and the 3′ strands labeled with fluorescein and Cy3, respectively.

Single-Molecule FRET Analysis

Fluorescence data at donor and acceptor wavelengths were acquired from single molecules by using a total internal reflection fluorescence microscope with 532 nm laser excitation and a back-illuminated EMCCD camera (iXON, Andor Technology). Microscope slides were successively treated with biotinylated BSA and streptavidin, and 50–250 pM fluorophore-labeled aptamer molecules were added to the slide. The data were acquired with integration times ranging from 16 to 100 ms depending on the sample dynamics. The base buffer used for imaging was 50 mM Tris-HCl (pH 8.1), 6% (w/w) glucose, 1% 2-mercaptoethanol, 0.1 mg/ml glucose oxidase (Sigma), 0.02 mg/ml glucose catalase (Sigma). Specified concentrations of $MgCl_2$ were included in the imaging buffer. Measurements were performed at room temperature (22°C). Single-molecule FRET efficiency after background correction was approximated by $(I_A/[I_A + I_D])$, where I_A and I_D are the fluorescence intensities of the acceptor and donor, respectively. Because the quantum yields and detection efficiencies of Cy3 and Cy5 are very close, E_{app} closely matches the true efficiency of energy transfer. Data analysis was carried out by using laboratory-written analysis routines developed in MATLAB 7. Single-molecule FRET histograms were obtained by averaging the first 10 frames of each FRET trace for every individual molecule after manually filtering photobleaching and blinking effects. States were identified from E_{app} histograms, and dwell times were analyzed if the time resolution allowed the clear observation of transitions. Rapidly fluctuating molecules undergo more transitions than slowly fluctuating ones, and thus in order to avoid bias toward fast rates, dwell time histograms were obtained by using a weighting factor inversely proportional to the number of transitions observed for each molecule. These dwell time histograms were then fitted to a single-exponential function to obtain the lifetimes of each state, the inverse of the rate of conversion. For the heterogeneity analysis, the average of the dwell times was calculated for each state for each individual molecule.

Partial RNase T1 Cleavage of RNA

[5′-^{32}P]RNA (final concentration < 1 nM) was incubated in a buffer containing 50 mM Tris-HCl (pH 8.3), 100 mM KCl in the absence or presence of 10 mM $MgCl_2$ and was incubated at 37°C for 5 min. RNase T1 (1 U) was then added and allowed to react for 2 min. Reactions were stopped by the addition of an equal volume of a solution of 97% formamide and 10 mM EDTA, and the products were separated on a 10% denaturing polyacrylamide gel. The gel was dried and exposed to Phosphor Imager screens.

Gel Electrophoresis under Nondenaturing Conditions

[5′-^{32}P]RNA (final concentration < 1 nM) in 90 mM Tris and 89 mM boric acid (pH ~8.5) (TB buffer) and 5 mM $MgCl_2$ was incubated at 37°C for 5 min before loading. RNA was electrophoresed in 8% acrylamide:bisacrylamide (29:1) gels in TB with $MgCl_2$ as required at room temperature at 100 V for 24 hr. The running buffer was circulated during electrophoresis. Dried gels were exposed to Phosphor Imager screens.

In-Line Probing of the *pbuE* Adenine Riboswitch Aptamer

[5′-^{32}P]RNA molecules (final concentration < 1 nM) were incubated for 48 hr at 25°C in a buffer containing 50 mM Tris-HCl (pH 8.3), 20 mM $MgCl_2$, and 100 mM KCl in the absence or presence of 10 μM ligand. At the end of each incubation, in-line probing cleavage products were separated by electrophoresis in 10% polyacrylamide gels containing 7 M urea. Dried gels were exposed to a storage phosphor screen and imaged (Bio-Rad).

In Vivo Analysis of *pbuE* Riboswitch Function

A pDG1661 plasmid containing the wild-type *pbuE* sequence comprising nucleotides −468 to +9 relative to the transcriptional start site of *pbuE* was kindly provided by R.R. Breaker (Yale University) [3]. Transformed *Bacillus subtilis* cells were grown to mid-exponential phase with constant shaking at 37°C in a minimal medium previously described [3]. Ligands were added to a final concentration of 0.5 mg/ml. Cells at the mid-exponential stage were harvested and resuspended in minimal medium in the presence or absence of ligands and were grown for an additional 3 hr, at which time 200 μl cell culture was assayed for β-galactosidase activity by using a variation of methods described by Mandal and Breaker [3].

Supplemental Data

Supplemental Data include two figures and are available at http://www.chembiol.com/cgi/content/full/13/8/857/DC1/.

Acknowledgments

We thank Ronald R. Breaker (Yale University) for discussion and for the generous gift of the pDG1661 plasmid, and we thank the National Sciences and Engineering Research Council of Canada (NSERC; grant to D.A.L.) and Cancer Research UK (grant to D.M.J.L.) for financial support. D.A.L. is a Chercheur-Boursier Junior I of the Fonds de la Recherche en Santé du Québec.

Received: April 13, 2006
Revised: June 1, 2006
Accepted: June 6, 2006
Published: August 25, 2006

References

1. Sudarsan, N., Barrick, J.E., and Breaker, R.R. (2003). Metabolite-binding RNA domains are present in the genes of eukaryotes. RNA *9*, 644–647.
2. Kubodera, T., Watanabe, M., Yoshiuchi, K., Yamashita, N., Nishimura, A., Nakai, S., Gomi, K., and Hanamoto, H. (2003). Thiamine-regulated gene expression of *Aspergillus oryzae* thiA requires splicing of the intron containing a riboswitch-like domain in the 5′-UTR. FEBS Lett. *555*, 516–520.
3. Mandal, M., and Breaker, R.R. (2004). Adenine riboswitches and gene activation by disruption of a transcription terminator. Nat. Struct. Mol. Biol. *11*, 29–35.
4. Soukup, J.K., and Soukup, G.A. (2004). Riboswitches exert genetic control through metabolite-induced conformational change. Curr. Opin. Struct. Biol. *14*, 344–349.
5. Mandal, M., Boese, B., Barrick, J.E., Winkler, W.C., and Breaker, R.R. (2003). Riboswitches control fundamental biochemical pathways in *Bacillus subtilis* and other bacteria. Cell *113*, 577–586.
6. Johansen, L.E., Nygaard, P., Lassen, C., Agerso, Y., and Saxild, H.H. (2003). Definition of a second *Bacillus subtilis* pur regulon comprising the pur and xpt-pbuX operons plus pbuG, nupG (yxjA), and pbuE (ydhL). J. Bacteriol. *185*, 5200–5209.
7. Nygaard, P., and Saxild, H.H. (2005). The purine efflux pump PbuE in *Bacillus subtilis* modulates expression of the PurR and G-box (XptR) regulons by adjusting the purine base pool size. J. Bacteriol. *187*, 791–794.
8. Serganov, A., Yuan, Y.R., Pikovskaya, O., Polonskaia, A., Malinina, L., Phan, A.T., Hobartner, C., Micura, R., Breaker, R.R., and Patel, D.J. (2004). Structural basis for discriminative regulation of gene expression by adenine- and guanine-sensing mRNAs. Chem. Biol. *11*, 1729–1741.
9. Batey, R.T., Gilbert, S.D., and Montange, R.K. (2004). Structure of a natural guanine-responsive riboswitch complexed with the metabolite hypoxanthine. Nature *432*, 411–415.
10. Lafontaine, D.A., Norman, D.G., and Lilley, D.M. (2002). The global structure of the VS ribozyme. EMBO J. *21*, 2461–2471.
11. Lafontaine, D.A., Norman, D.G., and Lilley, D.M. (2001). Structure, folding and activity of the VS ribozyme: importance of the 2-3-6 helical junction. EMBO J. *20*, 1415–1424.
12. Lescoute, A., and Westhof, E. (2006). Topology of three-way junctions in folded RNAs. RNA *12*, 83–93.
13. Orr, J.W., Hagerman, P.J., and Williamson, J.R. (1998). Protein and Mg^{2+}-induced conformational changes in the S15 binding site of 16 S ribosomal RNA. J. Mol. Biol. *275*, 453–464.
14. Noeske, J., Richter, C., Grundl, M.A., Nasiri, H.R., Schwalbe, H., and Wohnert, J. (2005). An intermolecular base triple as the basis of ligand specificity and affinity in the guanine- and adenine-sensing riboswitch RNAs. Proc. Natl. Acad. Sci. USA *102*, 1372–1377.
15. Wickiser, J.K., Cheah, M.T., Breaker, R.R., and Crothers, D.M. (2005). The kinetics of ligand binding by an adenine-sensing riboswitch. Biochemistry *44*, 13404–13414.
16. Ward, D.C., Reich, E., and Stryer, L. (1969). Fluorescence studies of nucleotides and polynucleotides. I. Formycin, 2-aminopurine riboside, 2,6-diaminopurine riboside, and their derivatives. J. Biol. Chem. *244*, 1228–1237.
17. Xu, D., Evans, K.O., and Nordlund, T.M. (1994). Melting and premelting transitions of an oligomer measured by DNA base fluorescence and absorption. Biochemistry *33*, 9592–9599.
18. Stivers, J.T. (1998). 2-Aminopurine fluorescence studies of base stacking interactions at abasic sites in DNA: metal-ion and base sequence effects. Nucleic Acids Res. *26*, 3837–3844.
19. Jean, J.M., and Hall, K.B. (2001). 2-Aminopurine fluorescence quenching and lifetimes: role of base stacking. Proc. Natl. Acad. Sci. USA *98*, 37–41.
20. Lafontaine, D.A., Wilson, T.J., Zhao, Z.Y., and Lilley, D.M. (2002). Functional group requirements in the probable active site of the VS ribozyme. J. Mol. Biol. *323*, 23–34.
21. Déclais, A.C., and Lilley, D.M. (2000). Extensive central disruption of a four-way junction on binding CCE1 resolving enzyme. J. Mol. Biol. *296*, 421–433.
22. Soukup, G.A., and Breaker, R.R. (1999). Relationship between internucleotide linkage geometry and the stability of RNA. RNA *5*, 1308–1325.
23. Nahvi, A., Sudarsan, N., Ebert, M.S., Zou, X., Brown, K.L., and Breaker, R.R. (2002). Genetic control by a metabolite binding mRNA. Chem. Biol. *9*, 1043.
24. Winkler, W., Nahvi, A., and Breaker, R.R. (2002). Thiamine derivatives bind messenger RNAs directly to regulate bacterial gene expression. Nature *419*, 952–956.
25. Winkler, W.C., and Breaker, R.R. (2003). Genetic control by metabolite-binding riboswitches. ChemBioChem *4*, 1024–1032.
26. Winkler, W.C., Cohen-Chalamish, S., and Breaker, R.R. (2002). An mRNA structure that controls gene expression by binding FMN. Proc. Natl. Acad. Sci. USA *99*, 15908–15913.
27. Winkler, W.C., Nahvi, A., Roth, A., Collins, J.A., and Breaker, R.R. (2004). Control of gene expression by a natural metabolite-responsive ribozyme. Nature *428*, 281–286.
28. Mandal, M., Lee, M., Barrick, J.E., Weinberg, Z., Emilsson, G.M., Ruzzo, W.L., and Breaker, R.R. (2004). A glycine-dependent riboswitch that uses cooperative binding to control gene expression. Science *306*, 275–279.
29. Law, S.M., Eritja, R., Goodman, M.F., and Breslauer, K.J. (1996). Spectroscopic and calorimetric characterizations of DNA duplexes containing 2-aminopurine. Biochemistry *35*, 12329–12337.
30. Khvorova, A., Lescoute, A., Westhof, E., and Jayasena, S.D. (2003). Sequence elements outside the hammerhead ribozyme catalytic core enable intracellular activity. Nat. Struct. Biol. *10*, 708–712.
31. Penedo, J.C., Wilson, T.J., Jayasena, S.D., Khvorova, A., and Lilley, D.M. (2004). Folding of the natural hammerhead ribozyme is enhanced by interaction of auxiliary elements. RNA *10*, 880–888.
32. Murchie, A.I., Thomson, J.B., Walter, F., and Lilley, D.M. (1998). Folding of the hairpin ribozyme in its natural conformation achieves close physical proximity of the loops. Mol. Cell *1*, 873–881.
33. Walter, N.G., Burke, J.M., and Millar, D.P. (1999). Stability of hairpin ribozyme tertiary structure is governed by the interdomain junction. Nat. Struct. Biol. *6*, 544–549.
34. Lilley, D.M. (1998). Folding of branched RNA species. Biopolymers *48*, 101–112.
35. Silverman, S.K., and Cech, T.R. (1999). Energetics and cooperativity of tertiary hydrogen bonds in RNA structure. Biochemistry *38*, 8691–8702.
36. Silverman, S.K., Zheng, M., Wu, M., Tinoco, I., Jr., and Cech, T.R. (1999). Quantifying the energetic interplay of RNA tertiary and secondary structure interactions. RNA *5*, 1665–1674.
37. Yamauchi, T., Miyoshi, D., Kubodera, T., Nishimura, A., Nakai, S., and Sugimoto, N. (2005). Roles of Mg^{2+} in TPP-dependent riboswitch. FEBS Lett. *579*, 2583–2588.
38. Lilley, D.M., and Wilson, T.J. (2000). Fluorescence resonance energy transfer as a structural tool for nucleic acids. Curr. Opin. Chem. Biol. *4*, 507–517.
39. Förster, T. (1948). Zwischenmolekulare Energiewanderung und Fluoreszenz. Ann. Phys. *2*, 55–75.
40. Norman, D.G., Grainger, R.J., Uhrin, D., and Lilley, D.M. (2000). Location of cyanine-3 on double-stranded DNA: importance for fluorescence resonance energy transfer studies. Biochemistry *39*, 6317–6324.

41. Hobartner, C., Rieder, R., Kreutz, C., Puffer, B., Lang, K., Polonskaia, A., Serganov, A., and Micura, R. (2005). Syntheses of RNAs with up to 100 nucleotides containing site-specific 2′-methylseleno labels for use in X-ray crystallography. J. Am. Chem. Soc. *127*, 12035–12045.
42. Sherlin, L.D., Bullock, T.L., Nissan, T.A., Perona, J.J., Lariviere, F.J., Uhlenbeck, O.C., and Scaringe, S.A. (2001). Chemical and enzymatic synthesis of tRNAs for high-throughput crystallization. RNA *7*, 1671–1678.
43. Lescoute, A., and Westhof, E. (2005). Riboswitch structures: purine ligands replace tertiary contacts. Chem. Biol. *12*, 10–13.
44. Mehta, A.D., Rief, M., Spudich, J.A., Smith, D.A., and Simmons, R.M. (1999). Single-molecule biomechanics with optical methods. Science *283*, 1689–1695.
45. Weiss, S. (2000). Measuring conformational dynamics of biomolecules by single molecule fluorescence spectroscopy. Nat. Struct. Biol. *7*, 724–729.
46. Zhuang, X., Bartley, L.E., Babcock, H.P., Russell, R., Ha, T., Herschlag, D., and Chu, S. (2000). A single-molecule study of RNA catalysis and folding. Science *288*, 2048–2051.
47. Zhuang, X., Kim, H., Pereira, M.J., Babcock, H.P., Walter, N.G., and Chu, S. (2002). Correlating structural dynamics and function in single ribozyme molecules. Science *296*, 1473–1476.
48. McKinney, S.A., Declais, A.C., Lilley, D.M., and Ha, T. (2003). Structural dynamics of individual Holliday junctions. Nat. Struct. Biol. *10*, 93–97.
49. Deniz, A.A., Laurence, T.A., Beligere, G.S., Dahan, M., Martin, A.B., Chemla, D.S., Dawson, P.E., Schultz, P.G., and Weiss, S. (2000). Single-molecule protein folding: diffusion fluorescence resonance energy transfer studies of the denaturation of chymotrypsin inhibitor 2. Proc. Natl. Acad. Sci. USA *97*, 5179–5184.
50. Schuler, B., Lipman, E.A., and Eaton, W.A. (2002). Probing the free-energy surface for protein folding with single-molecule fluorescence spectroscopy. Nature *419*, 743–747.
51. Rothwell, P.J., Berger, S., Kensch, O., Felekyan, S., Antonik, M., Wohrl, B.M., Restle, T., Goody, R.S., and Seidel, C.A. (2003). Multiparameter single-molecule fluorescence spectroscopy reveals heterogeneity of HIV-1 reverse transcriptase:primer/template complexes. Proc. Natl. Acad. Sci. USA *100*, 1655–1660.
52. Tan, E., Wilson, T.J., Nahas, M.K., Clegg, R.M., Lilley, D.M., and Ha, T. (2003). A four-way junction accelerates hairpin ribozyme folding via a discrete intermediate. Proc. Natl. Acad. Sci. USA *100*, 9308–9313.
53. Xie, Z., Srividya, N., Sosnick, T.R., Pan, T., and Scherer, N.F. (2004). Single-molecule studies highlight conformational heterogeneity in the early folding steps of a large ribozyme. Proc. Natl. Acad. Sci. USA *101*, 534–539.
54. Wickiser, J.K., Winkler, W.C., Breaker, R.R., and Crothers, D.M. (2005). The speed of RNA transcription and metabolite binding kinetics operate an FMN riboswitch. Mol. Cell *18*, 49–60.
55. Gusarov, I., and Nudler, E. (1999). The mechanism of intrinsic transcription termination. Mol. Cell *3*, 495–504.
56. Yakhnin, A.V., and Babitzke, P. (2002). NusA-stimulated RNA polymerase pausing and termination participates in the *Bacillus subtilis* trp operon attenuation mechanism in vitro. Proc. Natl. Acad. Sci. USA *99*, 11067–11072.
57. Milligan, J.F., Groebe, D.R., Witherell, G.W., and Uhlenbeck, O.C. (1987). Oligoribonucleotide synthesis using T7 RNA polymerase and synthetic DNA templates. Nucleic Acids Res. *15*, 8783–8798.
58. Pleiss, J.A., Derrick, M.L., and Uhlenbeck, O.C. (1998). T7 RNA polymerase produces 5′ end heterogeneity during in vitro transcription from certain templates. RNA *4*, 1313–1317.
59. Flannery, B.P., Teukolsky, S.A., and Vetterling, W.T. (1992). Numerical Recipes in Fortran, Second Edition (Cambridge, UK: Cambridge University Press).
60. Rist, M., and Marino, J. (2001). Association of an RNA kissing complex analyzed using 2-aminopurine fluorescence. Nucleic Acids Res. *29*, 2401–2408.
61. Wilson, T.J., and Lilley, D.M. (2002). Metal ion binding and the folding of the hairpin ribozyme. RNA *8*, 587–600.
62. Bassi, G.S., Murchie, A.I., Walter, F., Clegg, R.M., and Lilley, D.M. (1997). Ion-induced folding of the hammerhead ribozyme: a fluorescence resonance energy transfer study. EMBO J. *16*, 7481–7489.
63. Clegg, R.M., Murchie, A.I., Zechel, A., Carlberg, C., Diekmann, S., and Lilley, D.M. (1992). Fluorescence resonance energy transfer analysis of the structure of the four-way DNA junction. Biochemistry *31*, 4846–4856.
64. Murchie, A.I., Clegg, R.M., von Kitzing, E., Duckett, D.R., Diekmann, S., and Lilley, D.M. (1989). Fluorescence energy transfer shows that the four-way DNA junction is a right-handed cross of antiparallel molecules. Nature *341*, 763–766.